PAPER C

Synthesis Of Elastic Waves In Radially Layered Media With Horizontal structures

Youli Quan* and Xiaofei Chen**

ABSTRACT

The generalized reflection and transmission coefficients method with normal mode expansion is developed to calculate the elastic wave field for simulating energy propagation in sonic logging and the crosswell seismic data aquisition in complicated media. This method simulates models which consist of concentric cylindrical layers, and each cylindrical layer has within it horizontal layers in the z-direction. In the real world, the borehole casing with perforations, the source array, the open and cased boreholes embedded in layered media, etc. can be treated as this kind of model. The simulation based on this method gives reflections and transmissions, tube wave conversions generated at casing perforations and horizontal layers, the radiation pattern of a source array in a complicated borehole, and so on. This method is a semi-analytical approach. The calculation, therefore, is faster and more accurate than pure numerical methods. In this report we present five examples to show the possible applications of this approach. One of these examples is of special interest. In this example the borehole has a casing and the formation has a fault. We use this model to calculate a complete crosswell seismic data set which includes the borehole effects, reflections and scattering from the fault, tube waves, and other wave phenomena. This synthetic data set can be used to test tomography, reflection mapping and migration techniques. The computational time for this example is about 12 hours on a DEC alpha workstation.

---

* *STP, Stanford University*
** *Department of Earth Sciences, USC*

INTRODUCTION

For most borehole simulations (e.g., Tubman et al., 1984; Baker, 1984; Chen et al., 1994), a borehole is simply modeled as a series of concentric, cylindrical layers. In a real borehole, however, the medium within a cylindrical layer usually are not homogeneous, whose elastic parameters often change with depth. Pai et al. (1993) simulated the electromagnetic induction logging for this kind of models. For sonic logging problems we have to solve the elastodynamic equation in which both *P* and *S* waves are included. Therefore, the solutions for the elastic problem are more complex. For the elastic wave simulation, Bouchon (1993) presented a semi-analytical approach to use the boundary element method for a simple open borehole embedded in layered media. In this report we further develop the generalized reflection and transmission coefficients method (Chen et al., 1994) to calculate more realistic models, such as multi-layered boreholes (casing and invaded zones) embedded in multi-layered formation, faults in the formation, and perforation in a casing.

One of the objectives of this work is to calculate a complete crosswell seismic data set in which borehole effects, casing effects, tube waves, complex layers in formation, and so on, are included. Then, these synthetic data can be used to test tomography, reflection mapping and migration methods and programs.

PHYSICAL MODEL

Figure 1 shows a profile of a borehole model embedded in complex layered formation. The source is located inside the borehole, which can be a point source or finite cylinders. Receivers are located either inside or outside the borehole. This model looks complex, but it still has axially symmetric properties. Taking the advantage of this symmetry, we can derive a set of formulas to simulate the elastic wave propagation in this complex borehole-formation model.

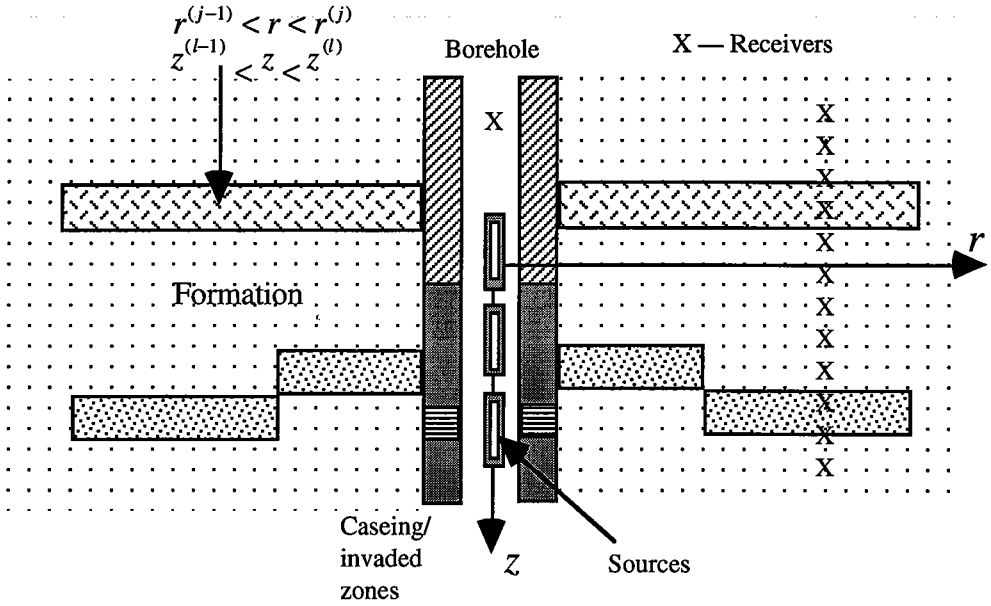

FIG. 1. A complicated borehole embedded in layered formation.

GOVERNING EQUATIONS

Since the model (see Figure 1) is independent of θ in cylindrical coordinates, we can write the displacement for the j^{th} cylindrical layer as

$$\mathbf{u}^{(j)} = \nabla\phi^{(j)} + \nabla\times(\mathbf{e}_\theta\psi^{(j)}). \tag{1}$$

The P wave potential $\phi^{(j)}$ and the S wave potential $\psi^{(j)}$ satisfy

$$\frac{\partial^2\phi^{(j)}(r,z)}{\partial r^2}+\frac{1}{r}\frac{\partial\,\phi^{(j)}(r,z)}{\partial r}+\frac{\partial^2\phi^{(j)}(r,z)}{\partial z^2}+k_\alpha^{(j)^2}(z)\phi^{(j)}(r,z)=F(\omega)\frac{\delta(r)\delta(z-z_s)}{2\pi r}, \tag{2a}$$

$$\frac{\partial^2\psi^{(j)}(r,z)}{\partial r^2}+\frac{1}{r}\frac{\partial\psi^{(j)}(r,z)}{\partial r}-\frac{\psi^{(j)}(r,z)}{r^2}+\frac{\partial^2\psi^{(j)}(r,z)}{\partial z^2}+k_\beta^{(j)^2}(z)\psi^{(j)}(r,z)=0, \tag{2b}$$

for $r^{(j-1)}<r<r^{(j)}$ (define $r^{(0)}=0$). Where, $F(\omega)$ is source function in frequency domain, z_s is the z coordinate of the source location, $k_\alpha^{(j)^2}(z)=\dfrac{\omega^2}{[\alpha^{(j)}(z)]^2}$ and $k_\beta^{(j)^2}(z)=\dfrac{\omega^2}{[\beta^{(j)}(z)]^2}$, here a and β are P and S velocities, respectively.

The potentials can be expanded by a set of eigen-functions, $\{f_n^{(j)}(z),\ g_n^{(j)}(z);\ n=1,2,...,N\}$, into

$$\phi^{(j)}(r,z)=\sum_{n=1}^{2N+1}\hat{\phi}_n^{(j)}(r)f_n^{(j)}(z), \tag{3a}$$

$$\psi^{(j)}(r,z)=\sum_{n=1}^{2N+1}\hat{\psi}_n^{(j)}(r)g_n^{(j)}(z). \tag{3b}$$

where the eigen-functions $f_n^{(j)}(z)$ and $g_n^{(j)}(z)$ satisfy

$$\frac{d^2f_n^{(j)}(z)}{dz^2}+[k_\alpha^{(j)}(z)]^2f_n^{(j)}(z)=[\gamma_n^{(j)}]^2f_n^{(j)}(z), \tag{4a}$$

$$\frac{d^2g_n^{(j)}(z)}{dz^2}+[k_\beta^{(j)}(z)]^2g_n^{(j)}(z)=[\nu_n^{(j)}]^2g_n^{(j)}(z). \tag{4b}$$

$\gamma_n^{(j)}$ and $\nu_n^{(j)}$ are the corresponding eigen-values to be determined. Solving equations (4a) and (4b) is an eigen-value problem. Precisely, equations (4a) and (4b) should be solved simultaneously by imposing the continuity of displacement and traction at each horizontal boundary, $z=z^{(j,l)}$,within *j*th cylindrical layer. If we solve them separately, the resulting eigen-functions will not include the *P-S* and *S-P* conversions at vertical boundaries. As an approximation for the situations where these conversions are not important, we solve them separately in this report. It should be pointed out that this approximation does not affect the existance of *P-S* and *S-P* conversions at boundaries $r=r^{(j)}$. Currently we are still working on this project and trying to overcome this limitation.

The detailed procedures of solving equation (4) will be described in a later section. The solutions are:

$$f_n^{(j)}(z)=\sum_{l=1}^{2N+1}a_p^{(j)}(l,n)\exp[ik_lz], \tag{5a}$$

$$g_n^{(j)}(z)=\sum_{l=1}^{2N+1}a_s^{(j)}(l,n)\exp[ik_lz], \tag{5b}$$

where $k_l=\pi(-l-N+1)/L$ for l=1, 2,..., 2N+1, and L is the periodic length (Chen et al., 1994). Substituting equation (3) into equation (2), we obtain

$$\sum_{n=1}^{2N+1}[\frac{d^2\hat{\phi}_n^{(j)}(r)}{dr^2}+\frac{1}{r}\frac{d\hat{\phi}_n^{(j)}(r)}{dr}+(\gamma_n^{(j)})^2\phi_n^{(j)}(r)]f_n^{(j)}(z)=F(\omega)\frac{\delta(r)\delta(z-z_s)}{2\pi r}, \tag{6a}$$

$$\sum_{n=1}^{2N+1}[\frac{d^2\hat{\psi}_n^{(j)}(r)}{dr^2}+\frac{1}{r}\frac{d\hat{\psi}_n^{(j)}(r)}{dr}-\frac{\hat{\psi}_n^{(j)}(r)}{r^2}+(\nu_n^{(j)})^2\hat{\psi}_n^{(j)}(r)]g_n^{(j)}(z)=0. \tag{6b}$$

Considering $\int_{-L/2}^{+L/2}f_n^{(j)}(z)f_m^{(j)*}(z)dz=\delta_{nm}$ and $\int_{-L/2}^{+L/2}g_n^{(j)}(z)g_m^{(j)*}(z)dz=\delta_{nm}$, we obtain

$$\frac{d^2\hat{\phi}_n^{(j)}(r)}{dr^2}+\frac{1}{r}\frac{d\hat{\phi}_n^{(j)}(r)}{dr}+(\gamma_n^{(j)})^2\phi_n^{(j)}(r)=F(\omega)\frac{\delta(r)]f_n^{(1)*}(z_s)}{2\pi r}, \tag{7a}$$

$$\frac{d^2\hat{\psi}_n^{(j)}(r)}{dr^2}+\frac{1}{r}\frac{d\hat{\psi}_n^{(j)}(r)}{dr}-\frac{\hat{\psi}_n^{(j)}(r)}{r^2}+(\nu_n^{(j)})^2\hat{\psi}_n^{(j)}(r)=0, \tag{7b}$$

where "*" means conjugate. The integral limits $\pm L/2$ define two artificial boundaries, which should be large enough so that the reflections from these artificial boundaries are out of the time window. The solutions of equation (7) are

$$\hat{\phi}_n^{(j)}=c_{p+}(n)H_o^{(1)}(\gamma_n^{(j)}r)+c_{p-}(n)H_o^{(2)}(\gamma_n^{(j)}r), \tag{8a}$$

$$\hat{\psi}_n^{(j)}=c_{s+}(n)H_1^{(1)}(\nu_n^{(j)}r)+c_{s-}(n)H_1^{(2)}(\nu_n^{(j)}r), \tag{8b}$$

for $j > 1$, and

$$\hat{\phi}_n^{(1)}=c(n)J_o(\gamma_n^{(1)}r)-\frac{iF(\omega)}{8\pi}f_n^{(1)*}H_o^{(1)}(\gamma_n^{(j)}r), \tag{8c}$$

$$\hat{\psi}_n^{(1)}=0, \tag{8d}$$

for $j = 1$ (fluid layer). Here, sign "+" refers to the wave going outward, and "-" refers to the wave coming inward. Coefficients $a_p^{(j)}(l,n)$ and $a_s^{(j)}(l,n)$ are orthonormal eigen-vectors corresponding to eigen-values $\gamma_n^{(j)}$ and $\nu_n^{(j)}$, respectively, and are given in a later section. Coefficients $c_{p\pm}$, $c_{s\pm}$, are determined by imposing boundary conditions at $r^{(j)}$, j=1,2, ..., J. Using the potentials, we obtain the displacements and stresses in the solid cylindrical layers ($j > 1$) as:

$$\begin{aligned}u_r^{(j)}(r,z)&=\frac{\partial\phi^{(j)}(r,z)}{\partial r}-\frac{\partial\psi^{(j)}(r,z)}{\partial z}\\&=\sum_{n=1}^{2N+1}[\frac{d\hat{\phi}_n^{(j)}}{dr}f_n^{(j)}(z)-\psi_n^{(j)}(r)\frac{dg_n^{(j)}}{dz}]\\&=\sum_{n=1}^{2N+1}\sum_{l=1}^{2N+1}[E_{11}^{(j)}(r;l,n)c_{p-}^{(j)}(n)+E_{12}^{(j)}(r;l,n)c_{s-}^{(j)}(n)\\&\qquad+E_{13}^{(j)}(r;l,n)c_{p+}^{(j)}(n)+E_{14}^{(j)}(r;l,n)c_{s+}^{(j)}(n)]\exp(ik_lz),\end{aligned} \tag{9a}$$

$$\begin{aligned}u_z^{(j)}(r,z)&=\frac{\partial\phi^{(j)}(r,z)}{\partial z}+\frac{1}{r}\frac{\partial[r\psi^{(j)}(r,z)]}{\partial r}\\&=\sum_{n=1}^{2N+1}[\hat{\phi}_n^{(j)}(r)\frac{df_n^{(j)}}{dz}+\frac{1}{r}\frac{d(r\psi_n^{(j)})}{dr}g_n^{(j)}(z)]\\&=\sum_{n=1}^{2N+1}\sum_{l=1}^{2N+1}[E_{21}^{(j)}(r;l,n)c_{p-}^{(j)}(n)+E_{22}^{(j)}(r;l,n)c_{s-}^{(j)}(n)\\&\qquad+E_{23}^{(j)}(r;l,n)c_{p+}^{(j)}(n)+E_{24}^{(j)}(r;l,n)c_{s+}^{(j)}(n)]\exp(ik_lz),\end{aligned} \tag{9b}$$

$$\sigma_r^{(j)}(r,z)=\lambda^{(j)}(z)\nabla^2\phi^{(1)}(r,z)+2\mu^{(j)}(z)[\frac{\partial^2\phi^{(j)}}{\partial r^2}-\frac{\partial^2\psi^{(j)}}{\partial r\partial z}]$$

$$= -(\lambda^{(j)} + 2\mu^{(j)})k_\alpha^{(j)}(z)\phi^{(j)}(r,z) - 2\mu^{(j)}[\frac{1}{r}\frac{\partial\phi^{(j)}(r,z)}{\partial r} + \frac{\partial^2\phi^{(j)}(r,z)}{\partial r^2} + \frac{\partial^2\psi}{\partial r\partial z}]$$

$$= \sum_{n=1}^{2N+1}\sum_{l=1}^{2N+1}[E_{31}^{(j)}(r;l,n)c_{p-}^{(j)}(n) + E_{32}^{(j)}(r;l,n)c_{s-}^{(j)}(n) + E_{33}^{(j)}(r;l,n)c_{p+}^{(j)}(n) + E_{34}^{(j)}(r;l,n)c_{s+}^{(j)}(n)]\exp(ik_l z), \quad (9c)$$

$$\sigma_z^{(j)}(r,z) = \mu^{(j)}(z)\{2\frac{\partial^2\phi^{(j)}}{\partial r\partial z} + \frac{\partial}{\partial r}[\frac{1}{r}\frac{\partial(r\psi^{(j)})}{\partial r}] - \frac{\partial^2\psi^{(j)}}{\partial z^2}\}$$

$$= 2\mu^{(j)})\{\frac{\partial^2\phi^{(j)}}{\partial r\partial z} - \frac{1}{2r}[k_\beta^{(j)}(z)]^2\psi^{(j)} - \frac{\partial^2\psi}{\partial z^2}\}$$

$$= \sum_{n=1}^{2N+1}\sum_{l=1}^{2N+1}[E_{41}^{(j)}(r;l,n)c_{p-}^{(j)}(n) + E_{42}^{(j)}(r;l,n)c_{s-}^{(j)}(n) + E_{43}^{(j)}(r;l,n)c_{p+}^{(j)}(n) + E_{44}^{(j)}(r;l,n)c_{s+}^{(j)}(n)]\exp(ik_l z), \quad (9d)$$

where $\{E_{pq}^{(j)}(r;l,n); p, q=1,2,3,4\}$ are given in the Appendix.

In the fluid-filled borehole (j=1), the displacement and stresses are:

$$u_r^{(1)}(r,z) = \frac{\partial\phi^{(1)}(r,z)}{\partial r}$$

$$= \sum_{n=1}^{2N+1}\sum_{l=1}^{2N+1}[E_{11}^{(1)}(r;l,n)c_{p-}^{(1)}(n) + E_{12}^{(1)}(r;l,n)c_{p+}^{(1)}(n)]\exp(ik_l z), \quad (10a)$$

$$\sigma_r^{(1)}(r,z) = \lambda^{(1)}(z)\nabla^2\phi^{(1)}(r,z)$$

$$= \sum_{n=1}^{2N+1}\sum_{l=1}^{2N+1}[E_{31}^{(1)}(r;l,n)c_{p-}^{(1)}(n) + E_{32}^{(1)}(r;l,n)c_{p+}^{(1)}(n)]\exp(ik_l z), \quad (10b)$$

$$\sigma_z^{(1)}(r,z) = 0, \quad (10c)$$

where, $s_+(n) = \frac{i}{8\pi}F(\omega)f_n^{(1)*}(z_s)$, and $\{E_{pq}^{(1)}(r;l,n); p$=1,2,3 and q=1,2$\}$ are given in the Appendix. Unknown coefficients $c_{p\pm}^{(j)}(n)$ and $c_{s\pm}^{(j)}(n)$ are determined by imposing boundary conditions at $r=r^{(j)}$, j=1, 2, ..., J. There are totally 4x(J+1)x(2N+1) unknown coefficients. The modified and generalized reflection and transmission (R/T) matrices are introduced to impose the boundary conditions.

MODIFIED R/T MATRICES

The modified R/T matrices, $\mathbf{R}_{-+}^{(j)}, \mathbf{R}_{+-}^{(j)}, \mathbf{T}_{+}^{(j)}$ and $\mathbf{T}_{-}^{(j)}$ at the interface $r=r^{(j)}$ are defined through relations

$$\begin{cases} \mathbf{C}_{+}^{(j+1)} = \mathbf{T}_{+}^{(j)}\mathbf{C}_{+}^{(j)} + \mathbf{R}_{-+}^{(j)}\mathbf{C}_{-}^{(j+1)} \\ \mathbf{C}_{-}^{(j)} = \mathbf{R}_{+-}^{(j)}\mathbf{C}_{+}^{(j)} + \mathbf{T}_{-}^{(j)}\mathbf{C}_{-}^{(j+1)} \end{cases} \tag{11a}$$

for $j>1$, and

$$\begin{cases} \mathbf{C}_{+}^{(2)} = \mathbf{T}_{+}^{(1)}(\mathbf{C}_{+}^{(1)} + \mathbf{s}_{+}) + \mathbf{R}_{-+}^{(1)}\mathbf{C}_{-}^{(2)} \\ \mathbf{C}_{-}^{(1)} = \mathbf{R}_{+-}^{(1)}(\mathbf{C}_{+}^{(1)} + \mathbf{s}_{+}) + \mathbf{T}_{-}^{(1)}\mathbf{C}_{-}^{(2)} \end{cases} \tag{11b}$$

for $j=1$, where $\mathbf{C}_{\pm}^{(j)} = [c_{p\pm}^{(j)}(1)\ c_{p\pm}^{(j)}(2)\ \ldots\ c_{p\pm}^{(j)}(2N+1)\ c_{s\pm}^{(j)}(1)\ c_{s\pm}^{(j)}(2)\ \ldots\ c_{s\pm}^{(j)}(2N+1)]^T$ are unknown coefficient vectors. These R/T matrices can be determined by imposing the boundary conditions at each radial boundary, $r = r^{(j)}$.

The boundary conditions for a solid-solid interface at $r=r^{(j)}$ ($j>1$) are:

$$u_r^{(j)}(r^{(j)},z) = u_r^{(j+1)}(r^{(j)},z), \tag{12a}$$
$$u_z^{(j)}(r^{(j)},z) = u_z^{(j+1)}(r^{(j)},z), \tag{12b}$$
$$\sigma_r^{(j)}(r^{(j)},z) = \sigma_r^{(j+1)}(r^{(j)},z), \tag{12c}$$
$$\sigma_z^{(j)}(r^{(j)},z) = \sigma_z^{(j+1)}(r^{(j)},z). \tag{12d}$$

Substituting equation (9) into equation (12) and operating $\int_{-L/2}^{+L/2}\exp(-ik_l z)dz$ on both sides, we obtain

$$[\mathbf{E}_{k1}^{(j)},\mathbf{E}_{k2}^{(j)}]\mathbf{C}_{-}^{(j)} + [\mathbf{E}_{k3}^{(j)},\mathbf{E}_{k4}^{(j)}]\mathbf{C}_{+}^{(j)} = [\mathbf{E}_{k1}^{(j+1)},\mathbf{E}_{k2}^{(j+1)}]\mathbf{C}_{-}^{(j+1)} + [\mathbf{E}_{k3}^{(j+1)},\mathbf{E}_{k4}^{(j+1)}]\mathbf{C}_{+}^{(j+1)}, \tag{13}$$

where k=1, 2, 3, 4. Comparing equations (11) and (13) we obtain

$$\begin{bmatrix} \mathbf{R}_{+-}^{(j)} & \mathbf{T}_{-}^{(j)} \\ \mathbf{T}_{+}^{(j)} & \mathbf{R}_{-+}^{(j)} \end{bmatrix} = \begin{bmatrix} \mathbf{E}_{11}^{(j)} & \mathbf{E}_{12}^{(j)} & -\mathbf{E}_{13}^{(j+1)} & -\mathbf{E}_{14}^{(j+1)} \\ \mathbf{E}_{21}^{(j)} & \mathbf{E}_{22}^{(j)} & -\mathbf{E}_{23}^{(j+1)} & -\mathbf{E}_{24}^{(j+1)} \\ \mathbf{E}_{31}^{(j)} & \mathbf{E}_{32}^{(j)} & -\mathbf{E}_{33}^{(j+1)} & -\mathbf{E}_{34}^{(j+1)} \\ \mathbf{E}_{41}^{(j)} & \mathbf{E}_{42}^{(j)} & -\mathbf{E}_{43}^{(j+1)} & -\mathbf{E}_{44}^{(j+1)} \end{bmatrix}^{-1} \begin{bmatrix} -\mathbf{E}_{13}^{(j)} & -\mathbf{E}_{14}^{(j)} & \mathbf{E}_{11}^{(j+1)} & \mathbf{E}_{12}^{(j+1)} \\ -\mathbf{E}_{23}^{(j)} & -\mathbf{E}_{24}^{(j)} & \mathbf{E}_{21}^{(j+1)} & \mathbf{E}_{22}^{(j+1)} \\ -\mathbf{E}_{33}^{(j)} & -\mathbf{E}_{34}^{(j)} & \mathbf{E}_{31}^{(j+1)} & \mathbf{E}_{32}^{(j+1)} \\ -\mathbf{E}_{43}^{(j)} & -\mathbf{E}_{44}^{(j)} & \mathbf{E}_{41}^{(j+1)} & \mathbf{E}_{42}^{(j+1)} \end{bmatrix}_{r=r^{(j)}}, \tag{14}$$

for j>1, where $\mathbf{T}_{+}$, $\mathbf{T}_{-}$, $\mathbf{R}_{-+}$ and $\mathbf{R}_{+-}$ are (4N+2)x(4N+2) matrices, and $\mathbf{E}_{pq}^{(j)}$ are (2N+1) x(2N+1) matrices.

The boundary conditions at liquid-solid interface $r = r^{(1)}$ are

$$u_r^{(1)}(r^{(1)},z) = u_r^{(2)}(r^{(1)},z), \tag{15a}$$
$$\sigma_r^{(1)}(r^{(1)},z) = \sigma_r^{(2)}(r^{(1)},z), \tag{15b}$$
$$0 = \sigma_z^{(2)}(r^{(1)},z). \tag{15c}$$

Similarly, using equations (10), (11b) and (15) we obtain the modified R/T matrices for the first layer as

$$\begin{bmatrix} \mathbf{R}_{+-}^{(1)} & \mathbf{T}_{-}^{(1)} \\ \mathbf{T}_{+}^{(1)} & \mathbf{R}_{-+}^{(1)} \end{bmatrix} = \begin{bmatrix} \mathbf{E}_{11}^{(1)} & -\mathbf{E}_{13}^{(2)} & -\mathbf{E}_{14}^{(2)} \\ \mathbf{E}_{31}^{(1)} & -\mathbf{E}_{33}^{(2)} & -\mathbf{E}_{34}^{(2)} \\ \mathbf{0} & -\mathbf{E}_{43}^{(2)} & -\mathbf{E}_{44}^{(2)} \end{bmatrix}^{-1} \begin{bmatrix} -\mathbf{E}_{13}^{(1)} & \mathbf{E}_{11}^{(2)} & \mathbf{E}_{12}^{(2)} \\ -\mathbf{E}_{33}^{(1)} & \mathbf{E}_{31}^{(2)} & \mathbf{E}_{32}^{(2)} \\ \mathbf{0} & \mathbf{E}_{41}^{(2)} & \mathbf{E}_{42}^{(2)} \end{bmatrix}_{r=r^{(1)}}, \tag{16}$$

where, $\mathbf{T}_{-}^{(1)}$, $\mathbf{T}_{+}^{(1)}$, $\mathbf{R}_{+-}^{(1)}$ and $\mathbf{R}_{-+}^{(1)}$ are $(2N+1)\mathrm{x}(4N+2)$, $(4N+2)\mathrm{x}(2N+1)$, $(2N+1)\mathrm{x}(2N+1)$ and $(4N+2)\mathrm{x}(4N+2)$ matrices, respectively.

GENERALIZED R/T MATRICES

The generalized R/T matrices $\hat{\mathbf{R}}_{+-}^{(j)}$ and $\hat{\mathbf{T}}_{+}^{(j)}$ are introduced via relations

$$\begin{cases} \mathbf{C}_{+}^{(j+1)} = \hat{\mathbf{T}}_{+}^{(j)} \mathbf{C}_{+}^{(j)} \\ \mathbf{C}_{-}^{(j)} = \hat{\mathbf{R}}_{+-}^{(j)} \mathbf{C}_{+}^{(j)} \end{cases}, \tag{17a}$$

for $j>1$, and

$$\begin{cases} \mathbf{C}_{+}^{(2)} = \hat{\mathbf{T}}_{+}^{(1)} (\mathbf{C}_{+}^{(1)} + \mathbf{s}_{+}) \\ \mathbf{C}_{-}^{(1)} = \hat{\mathbf{R}}_{+-}^{(1)} (\mathbf{C}_{+}^{(1)} + \mathbf{s}_{+}) \end{cases} \tag{17b}$$

for $j=1$. Substituting equation (17) into equation (12) and rearranging terms, we obtain a recursive relation

$$\begin{cases} \hat{\mathbf{T}}_{+}^{(j)} = [\mathbf{I} - \mathbf{R}_{-+}^{(j)} \hat{\mathbf{R}}_{+-}^{(j+1)}]^{-1} \mathbf{T}_{+}^{(j)} \\ \hat{\mathbf{R}}_{+-}^{(j)} = \mathbf{R}_{+-}^{(j)} + \mathbf{T}_{-}^{(j)} \hat{\mathbf{R}}_{+-}^{(j+1)} \hat{\mathbf{T}}_{+}^{(j)} \end{cases}, \qquad \text{for } j = J, J\text{-}1, \ldots, 2,1, \tag{18}$$

where $\mathbf{I}$ is the unit matrix, $\hat{\mathbf{R}}_{+-}^{(j)}$ and $\hat{\mathbf{T}}_{+}^{(j)}$ are $(4N+2)\mathrm{x}(4N+2)$ matrices for $j > 1$, $\hat{\mathbf{T}}_{+}^{(1)}$ is a $(4N+2)\mathrm{x}(2N+1)$ matrix, and $\hat{\mathbf{R}}_{+-}^{(1)}$ is a $(2N+1)\mathrm{x}(2N+1)$ matrix. In the outer most layer ($j = N+1$), there exist only outward-going waves, i.e., $\mathbf{C}_{-}^{(N+1)} = \mathbf{0}$. Therefore, the initial condition for the iteration is

$$\hat{\mathbf{R}}_{+-}^{(N+1)} = \mathbf{0}. \tag{19}$$

Using equation (18), with initial condition (19), we can recursively calculate the generalized R/T matrices $\hat{\mathbf{R}}_{+-}^{(j)}$ and $\hat{\mathbf{T}}_{+}^{(j)}$ for all interfaces from modified R/T matrices $\mathbf{T}_{+}^{(j)}$, $\mathbf{T}_{-}^{(j)}$, $\mathbf{R}_{-+}^{(j)}$ and $\mathbf{R}_{+-}^{(j)}$ calculated by equations (14) and (16).

FINAL SOLUTIONS

Using the generalized R/T matrices we can easily obtain the coefficient vectors $\mathbf{C}_{\pm}^{(j)}$. Inside the first layer (j=1) we have

$$\mathbf{C}_{+}^{(1)} = \mathbf{C}_{-}^{(1)} \tag{20}$$

where the relation $J_o = \frac{1}{2}(H_o^{(2)} + H_o^{(1)})$ is used. Substituting (20) into (17b) yields

$$\mathbf{C}_{+}^{(1)} + \mathbf{s}_{+} = (\mathbf{I} - \mathbf{R}_{+-}^{(1)})^{-1}\mathbf{s}_{+}. \tag{21}$$

Then, substituting (21) into (17a) we have

$$\begin{cases} \mathbf{C}_{+}^{(j)} = \hat{\mathbf{T}}_{+}^{(j-1)}\hat{\mathbf{T}}_{+}^{(j-2)}\ldots\hat{\mathbf{T}}_{+}^{(1)}(\mathbf{I} - \hat{\mathbf{R}}_{+-}^{(1)})^{-1}s_{+} \\ \mathbf{C}_{-}^{(j)} = \hat{\mathbf{R}}_{+-}^{(j)}\mathbf{C}_{+}^{(j)} \end{cases}. \tag{22}$$

Once having the coefficients $\mathbf{C}_{\pm}$ we can calculate the frequency domain solutions (displacements and stresses) using equations (9) and (10). The corresponding time domain solution can be obtained by performing inverse Fourier transform.

SOLUTIONS FOR $f_n^{(j)}(z)$ *and* $g_n^{(j)}(z)$

In this section, we shall solve equation (4). Namely, determine $\{\gamma_n^{(j)},\ \nu_n^{(j)}\}$ appeared in equation (4) and $\{a_p^{(j)}(l,n),\ a_s^{(j)}(l,n)\}$ in equation (5). This is an eigen-value problem. Substituting equation (5) into equation (4), we have

$$\sum_{l=1}^{2N+1}\{-(k_l)^2 + [k_\alpha^{(j)}(z)]^2 - (\gamma_n^{(j)})^2\}a_p^{(j)}(l,n)\exp(ik_l z) = 0, \tag{23a}$$

$$\sum_{l=1}^{2N+1}\{-(k_l)^2 + [k_\beta^{(j)}(z)]^2 - (\nu_n^{(j)})^2\}a_s^{(j)}(l,n)\exp(ik_l z) = 0. \tag{23b}$$

Operating $\int_{-L/2}^{+L/2}\exp(-ik_m z)dz$ on equation (23), we obtain the following compact matrix equations,

$$[\mathbf{A}^{(j)} - (\gamma_n^{(j)})^2\mathbf{I}]\mathbf{a}_p^{(j)}(n) = 0, \tag{24a}$$

$$[\mathbf{B}^{(j)} - (\nu_n^{(j)})^2\mathbf{I}]\mathbf{a}_s^{(j)}(n) = 0, \tag{24b}$$

where,

$$\mathbf{a}_p^{(j)}(n) = [a_p^{(j)}(1,n), a_p^{(j)}(2,n),\ldots, a_p^{(j)}(2N+1,n)]^T,$$

$$\mathbf{a}_s^{(j)}(n) = [a_s^{(j)}(1,n), a_s^{(j)}(2,n),\ldots, a_s^{(j)}(2N+1,n)]^T,$$

$$A_{ml}^{(j)} = -(k_m)^2 \delta_{lm} + \int_{-L/2}^{+L/2} [k_\alpha^{(j)}(z)]^2 \exp[i(k_l - k_m)z]dz, \quad (25a)$$

$$B_{ml}^{(j)} = -(k_m)^2 \delta_{lm} + \int_{-L/2}^{+L/2} [k_\beta^{(j)}(z)]^2 \exp[i(k_l - k_m)z]dz. \quad (25b)$$

Eigen-values $(\gamma_n^{(j)})^2$ and $(\nu_n^{(j)})^2$, and their related eigen-vectors $\mathbf{a}_p^{(j)}(n)$ and $\mathbf{a}_s^{(j)}(n)$ are calculated using standard linear algebra programs. Here, $L = z_m - z_o$ is periodic length that is as the distance between two artificial boundaries.

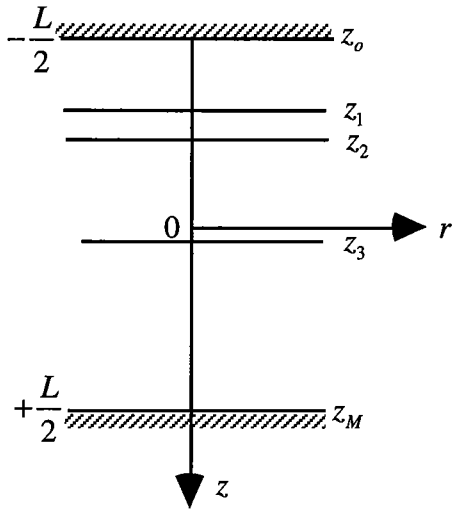

FIG. 2. A model of vertically layered media. In order to treat it as a eigen-value problem, two artificial boundaries z_o and z_N are added.

Let us consider a special case: homogeneous layer (i.e., $k_\alpha^{(j)}(z) = k_\alpha^{(j)}$, and $k_\beta^{(j)}(z) = k_\beta^{(j)}$). For this case, we have obtained the semi-analytical solution in a previous study (Chen et al., 1994). From equations (24) and (25) we simply obtain

$$(\gamma_n^{(j)})^2 = (k_\alpha^{(j)})^2 - k_n^2, \quad (26a)$$

$$a_p^{(j)}(l,n) = \delta_{ln}, \quad (26b)$$

and

$$(\nu_n^{(j)})^2 = (k_\beta^{(j)})^2 - k_n^2, \quad (27a)$$

$$a_s^{(j)}(l,n) = \delta_{ln}. \quad (27b)$$

Substituting these special solutions into equations (9) and (10), we obtain the identical formulas with the semi-analytic solutions of Chen et al (1994).

For the case of M vertical layers (i.e., $k_{\alpha_{(i)}}^{(j)}(z) = k_{\alpha_{(i)}}^{(j)}$ and $k_{\beta_{(i)}}^{(j)}(z) = k_{\beta_{(i)}}^{(j)}$, for $z_i^{(j-1)} < z < z_i^{(j)}$, $i = 1,2,...,M$), the integral in equation (25) can be written as

$$\int_{-L/2}^{+L/2}[k_\alpha^{(j)}(z)]^2 e^{i(k_l-k_m)}dz = \sum_{i=1}^{M}\{(k_{\alpha_i}^{(j)})^2 e^{i(k_l-k_m)(z_{i-1}+d_i)}\frac{2\sin[(k_l-k_m)d_i]}{k_l-k_m}\}, \quad (28a)$$

$$\int_{-L/2}^{+L/2}[k_\beta^{(j)}(z)]^2 e^{i(k_l-k_m)}dz = \sum_{i=1}^{M}\{(k_{\beta_i}^{(j)})^2 e^{i(k_l-k_m)(z_{i-1}+d_i)}\frac{2\sin[(k_l-k_m)d_i]}{k_l-k_m}\}, \quad (28b)$$

where $d_i = (z_i - z_{i-1})/2$.

The discrete wavenumber method is used for implementation. In the numerical computation, the following rules are applied to select the parameters: $k_{\max} > \omega / \min(\beta_i^{(j)})$, $k_{\max} > \pi / \min(d_i)$, $\Delta k = \pi / L$ and $k_m = -k_{\max} + m\Delta k$, where k_{max} determine the upper limit of the summation over k in equations (9) and (10); Δk is the increment of wavenumber.

EXAMPLES

We present five examples to show the capabilities of this method. Figure 3 is the simulation of sonic logging. There is a high velocity layer in the formation. The moveout of the *P* and *S* waves is changed by the high velocity zone. This test shows that the frequency can be up to 20 KHz (the central frequency is 10KHz) in the simulation. Figures 4 – 7 are crosswell profiling examples. In these examples the seismograms are of the U_r component. Figure 4 shows the simulation of a fluid-filled open borehole. The formation has a low velocity layer which exhibits a significant influence on the wave field. The tube wave converts to *P* and *S* waves at the boundaries. The wave field within the low velocity zone is very complicated. Figure 5 gives an example of cased borehole. To simulate how a perforation in a casing creates tube conversions, we put a low velocity layer in the casing. The tube wave to *P* and *S* wave conversions clearly show up. Figure 6 is a cased borehole embedded in a multi-layered formation. There is a low velocity layer and a high velocity layer. Though the low velocity zone is only 1 m thick, its effects on the wave field can be clearly seen. Figure 7 is a common receiver gather sorted from a complete crosswell data set. There are 50 sources and 50 receivers. The source interval and receiver interval are all 2 m. The moveout of the tube wave in a common receiver gather is very different from that in a common source gather. In this example we include a cased borehole and a layer with a fault. We are going to use this synthetic data set to test tomography techniques and other inversion methods. These kinds of tests help us to understand the borehole effects on the inversion.

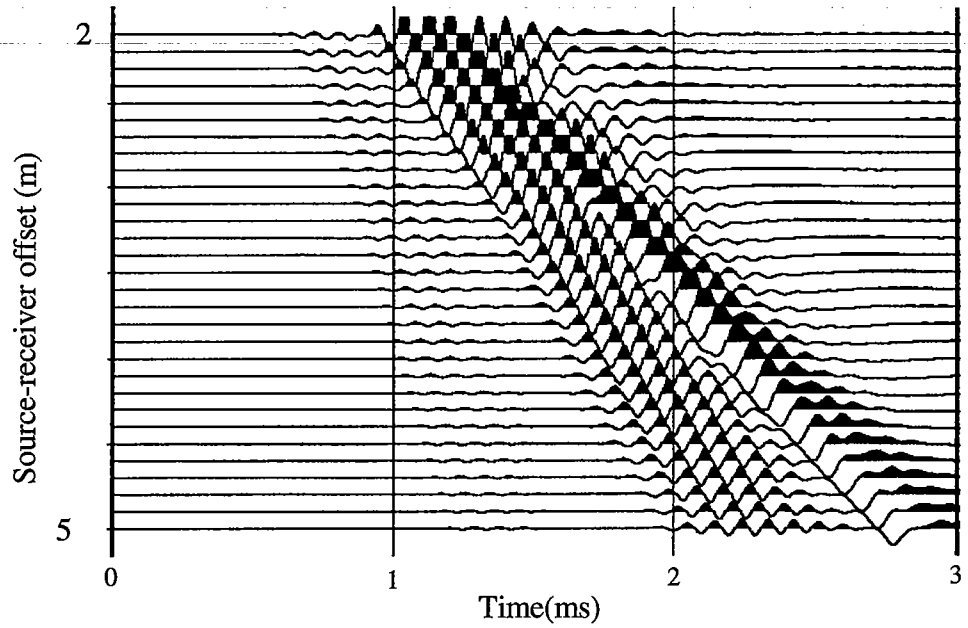

(a) Synthetic full waveform sonic log. The center frequency of the source wavelet is 10 KHz.

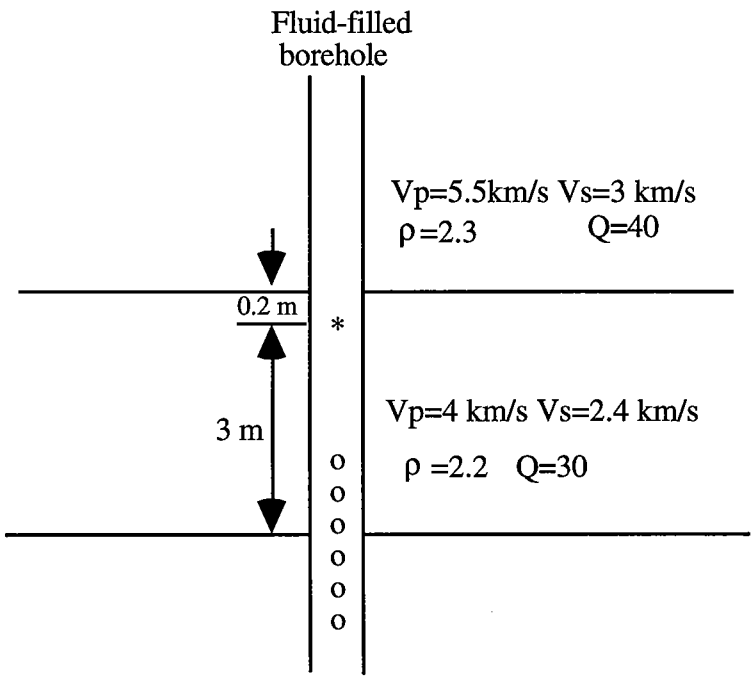

(b) Model used to calculate the sonic log shown in (a).

FIG. 3. Simulation of sonic log in a layered medium.

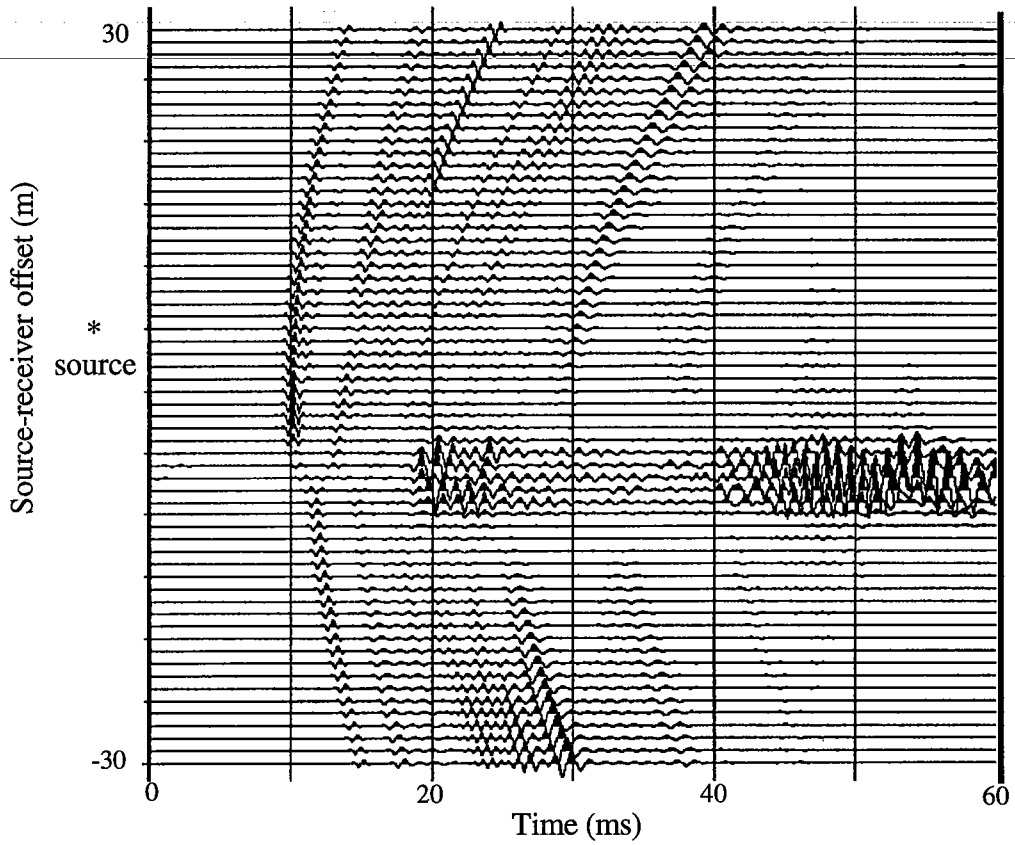

(a) A common source gather of crosswell survey using the model in (b). The center frequency of the source wavelet is 1 KHz.

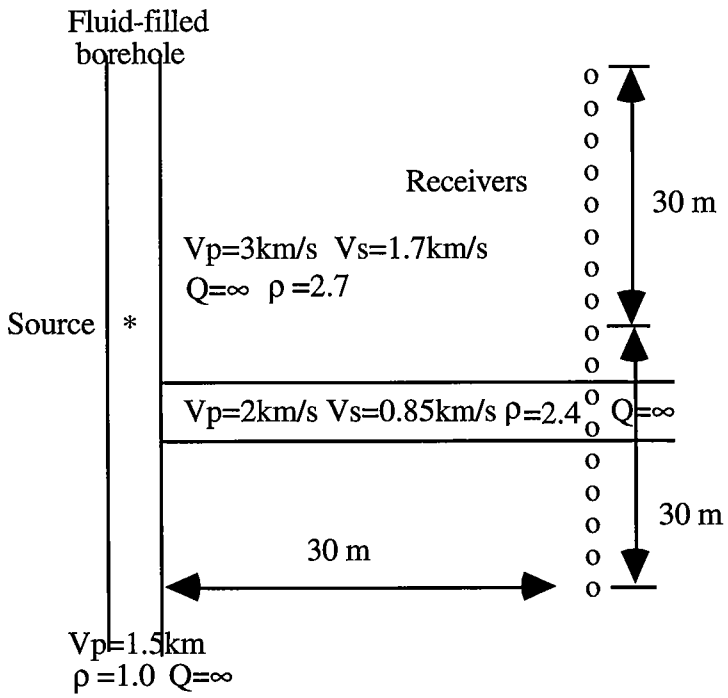

(b) model geometry and parameters

FIG. 4. Simulation of crosswell for open borehole in the formation with low velocity zone.

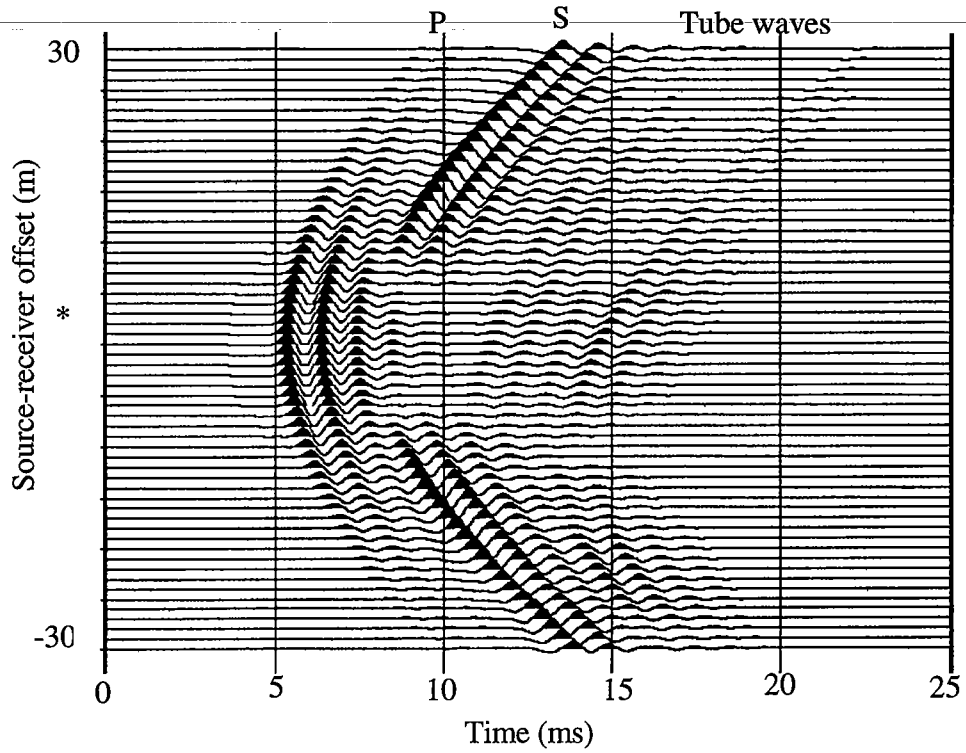

(a) Seismograms. The center frequency of the source wavelet is 1 KHz.

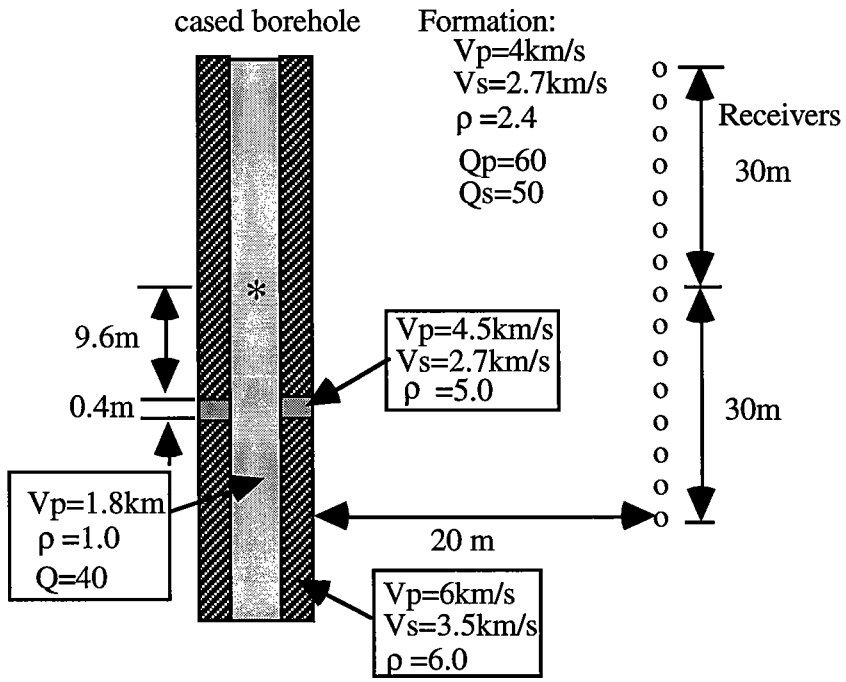

(b) Model geometry and parameters.

FIG. 5. Test on the effect of casing perforation. It can be seen that the tube wave converts to *P* and *S* waves at a perforation..

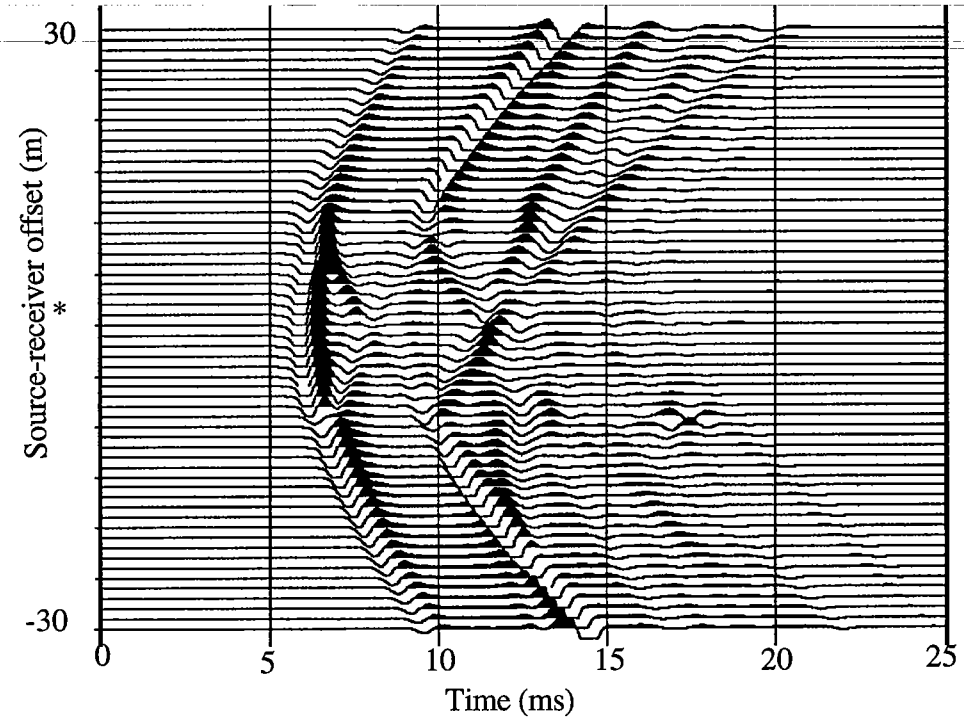

(a) Seismograms. The center frequency of the source wavelet is 1 KHz.

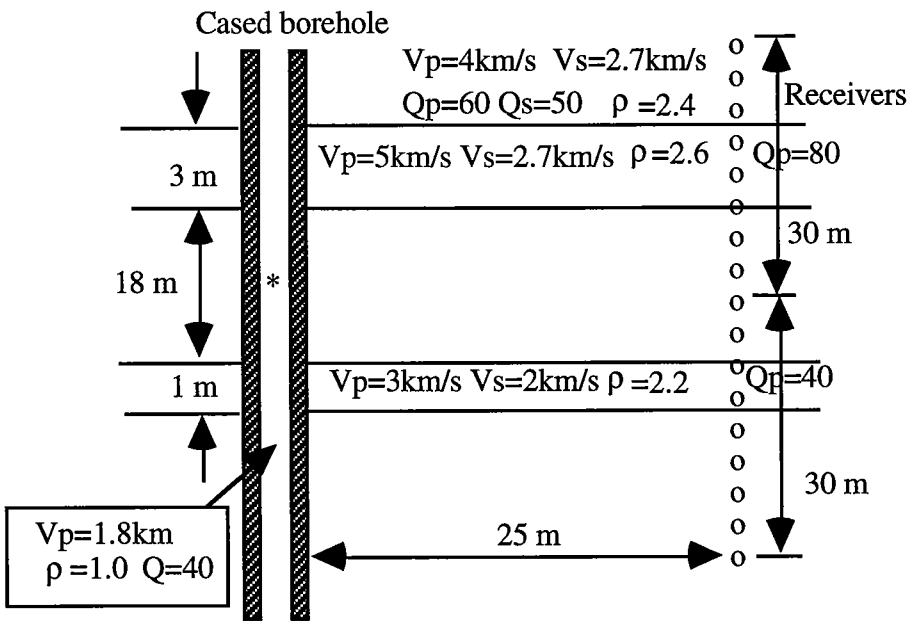

(b) Model geometry and parameters.

FIG. 6. Simulation for a cased borehole embeds in a formation with multi-layers.

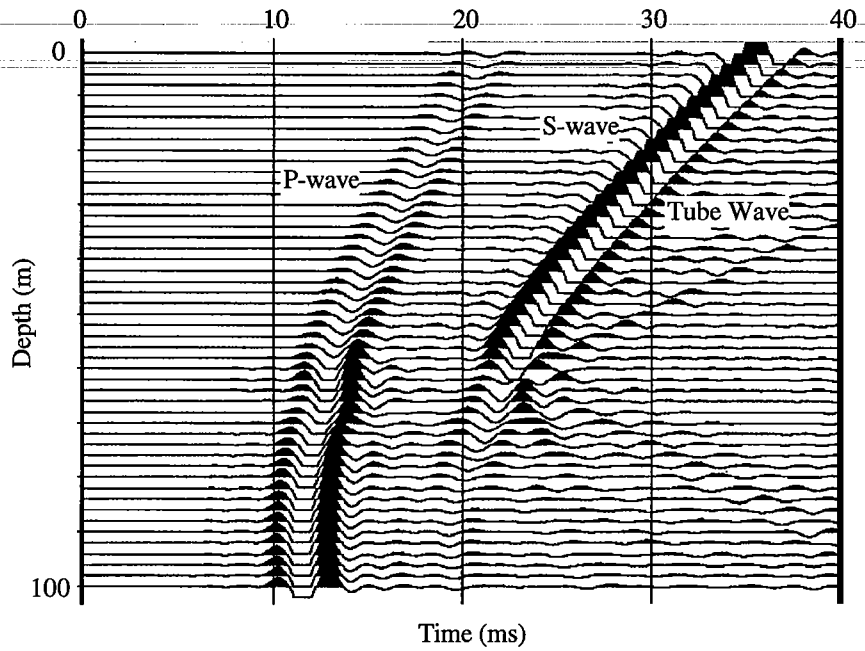

(a) seismograms. The center frequency is 300 Hz.

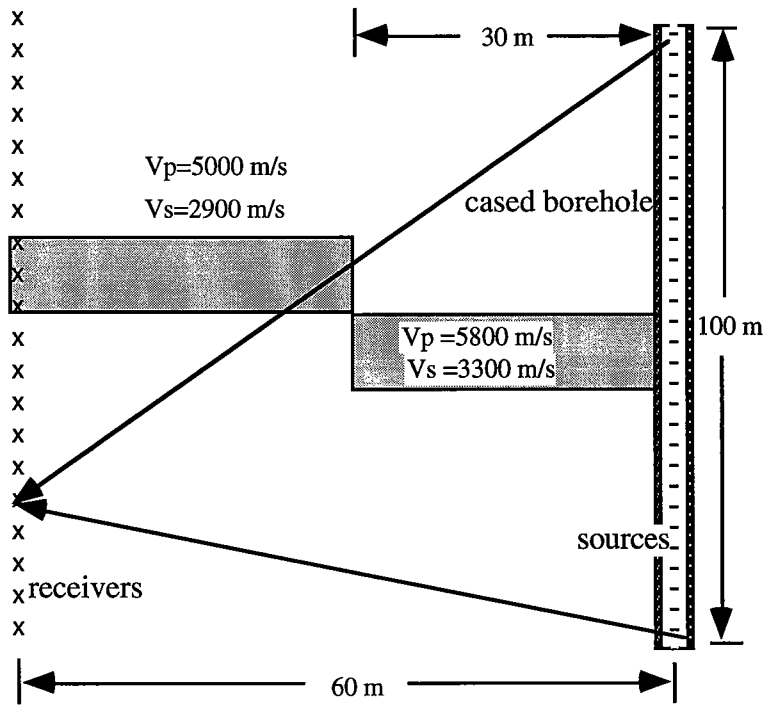

(b) Model geometry and parameters.

FIG. 7. A common receiver gather sorted from a complete synthetic crosswell data set.

CONCLUSION

We have developed a semi-analytical approach to simulate the waves in a complex borehole-formation model in which there exist both cylindrical and horizontal layers. In this approach, we first calculate the eigen-functions of horizontal layers for each cylindrical layer. Then, we expand the wave equation solutions into these eigen-functions and apply the generalized reflection and transmission coefficients method to solve the boundary problem for radial layers. Numerical examples show that this approach provides an effective tool to simulate complex models which are found in sonic logging and crosswell seismic profiling. Since we neglect the *P-S* and *S-P* conversions due to the *horizontal interfaces,* this approach is valid for the cases in which those conversions are not important. Currently, we are still working on this project, and we hope to obtain a complete solution.

REFERENCES

Baker, L., J., 1984, The effect of the invaded zone on the full wavetrain acoustic logging: Geophysics, **49**, 789.

Bouchon, M., 1993, A numerical simulation of the acoustic and elastic wavefields radiated by a source on a fluid-filled borehole embedded in layered medium: Geophysics, **58**, No. 4, 475-481.

Chen, X, Quan, Y and Harris, M. J., 1994, Seismogram synthesis for radially layered media using the generalized reflection/transmission coefficients method: Expanded Abstracts of the 64th SEG annual meeting.

Pai, D. M., Ahmad, J. and Kennedy W. D., 1993, Two-dimensional induction log modeling using a coupled-mode, multiple-reflection series method: Geophysics, **58**, No. 4, 466-474.

Tubman, K. M., Cheng, C. H. and Toksöz, M. N., 1984, Synthetic full waveform acoustic logs in cased boreholes: Geophysics, **49**, 1051-1059.

APPENDIX

For j>1 the elements E_{pq} in equation (9) are:

$$
\begin{aligned}
E_{11}^{(j)}(r;l,n) &= -\gamma_n^{(j)} H_1^{(2)}(\gamma_n^{(j)} r) a_p^{(j)}(l,n), \\
E_{12}^{(j)}(r;l,n) &= -ik_t H_1^{(2)}(\nu_n^{(j)} r) a_s^{(j)}(l,n), \\
E_{13}^{(j)}(r;l,n) &= -\gamma_n^{(j)} H_1^{(1)}(\gamma_n^{(j)} r) a_p^{(j)}(l,n), \\
E_{14}^{(j)}(r;l,n) &= -ik_t H_1^{(1)}(\nu_n^{(j)} r) a_s^{(j)}(l,n), \\
E_{21}^{(j)}(r;l,n) &= ik_t H_o^{(2)}(\gamma_n^{(j)} r) a_p^{(j)}(l,n), \\
E_{22}^{(j)}(r;l,n) &= \nu_n^{(j)} H_o^{(2)}(\nu_n^{(j)} r) a_s^{(j)}(l,n), \\
E_{23}^{(j)}(r;l,n) &= ik_t H_o^{(1)}(\gamma_n^{(j)} r) a_p^{(j)}(l,n), \\
E_{22}^{(j)}(r;l,n) &= \nu_n^{(j)} H_o^{(1)}(\nu_n^{(j)} r) a_s^{(j)}(l,n),
\end{aligned}
$$

$$E_{31}^{(j)}(r;l,n)=\sum_{m=1}^{2N+1}\{[2k_m^2H_o^{(2)}(\gamma_n^{(j)}r)+\frac{2\gamma_n^{(j)}}{r}H_1^{(2)}(\gamma_n^{(j)}r)]\mu_{lm}^{(j)}a_p^{(j)}(m,,n)$$
$$-\omega^2H_o^{(2)}(\gamma_n^{(j)}r)\rho_{lm}^{(j)}a_p^{(j)}(m,n)\},$$

$$E_{32}^{(j)}(r;l,n)=\sum_{m=1}^{2N+1}[-i2k_m\nu_n^{(j)}\dot{H}_1^{(2)}(\nu_n^{(j)}r)\mu_{lm}^{(j)}a_s^{(j)}(m,n),$$

$$E_{33}^{(j)}(r;l,n)=\sum_{m=1}^{2N+1}\{[2k_m^2H_o^{(1)}(\gamma_n^{(j)}r)+\frac{2\gamma_n^{(j)}}{r}H_1^{(2)}(\gamma_n^{(j)}r)]\mu_{lm}^{(j)}a_p^{(j)}(m,,n)$$
$$-\omega^2H_o^{(1)}(\gamma_n^{(j)}r)\rho_{lm}^{(j)}a_p^{(j)}(m,n)\},$$

$$E_{34}^{(j)}(r;l,n)=\sum_{m=1}^{2N+1}[-i2k_m\nu_n^{(j)}\dot{H}_1^{(1)}(\nu_n^{(j)}r)\mu_{lm}^{(j)}a_s^{(j)}(m,n)],$$

$$E_{41}^{(j)}(r;l,n)=\sum_{m=1}^{2N+1}[-i2k_m\gamma_n^{(j)}H_1^{(2)}(\gamma_n^{(j)}r)\mu_{lm}^{(j)}a_p^{(j)}(m,n)],$$

$$E_{42}^{(j)}(r;l,n)=\sum_{m=1}^{2N+1}[2k_m^2\mu_{lm}^{(j)}-\omega^2\rho_{lm}^{(j)}]H_1^{(2)}(\nu_n^{(j)}r)a_s^{(j)}(m,n),$$

$$E_{43}^{(j)}(r;l,n)=\sum_{m=1}^{2N+1}[-i2k_m\gamma_n^{(j)}H_1^{(1)}(\gamma_n^{(j)}r)\mu_{lm}^{(j)}a_p^{(j)}(m,n)],$$

$$E_{44}^{(j)}(r;l,n)=\sum_{m=1}^{2N+1}[2k_m^2\mu_{lm}^{(j)}-\omega^2\rho_{lm}^{(j)}]H_1^{(1)}(\nu_n^{(j)}r)a_s^{(j)}(m,n),$$

where $\mu_{lm}^{(j)}=\int_{-L/2}^{+L/2}\mu^{(j)}(z)\exp[i(k_l-k_m)z]dz$ and $\rho_{lm}^{(j)}=\int_{-L/2}^{+L/2}\rho^{(j)}(z)\exp[i(k_l-k_m)z]dz$.

For j=1 the elements E_{pq} in equation (10) are:

$$E_{11}^{(1)}(r;l,n)=-\gamma_n^{(1)}H_1^{(2)}(\gamma_n^{(1)}r)a_p^{(1)}(l,n),$$
$$E_{12}^{(1)}(r;l,n)=-\gamma_n^{(1)}H_1^{(1)}(\gamma_n^{(1)}r)a_p^{(1)}(l,n),$$
$$E_{21}^{(1)}(r;l,n)=ik_lH_o^{(2)}(\gamma_n^{(1)}r)a_p^{(1)}(l,n),$$
$$E_{22}^{(j)}(r;l,n)=ik_lH_o^{(1)}(\gamma_n^{(j)}r)a_p^{(j)}(l,n),$$
$$E_{31}^{(1)}(r;l,n)=-\lambda^{(1)}(k_\alpha^{(1)})^2H_o^{(2)}(\gamma_n^{(1)}r)a_p^{(1)}(l,n),$$
$$E_{32}^{(1)}(r;l,n)=-\lambda^{(1)}(k_\alpha^{(1)})^2H_o^{(1)}(\gamma_n^{(1)}r)a_p^{(1)}(l,n).$$